AGU ADVANCING EARTH AND SPACE SCIENCE

Geophysical Research Letters®

RESEARCH LETTER
10.1029/2022GL102312

Terrestrial Heat Flow Variation With Depth Caused by Anomalously High Radiogenic Heat Production

Yibo Wang[1,2], Kevin Furlong[3], Sven Fuchs[2], Lijuan He[1,4], and Shengbiao Hu[1,4]

[1]State Key Laboratory of Lithospheric Evolution, Institute of Geology and Geophysics Chinese Academy of Sciences, Beijing, China, [2]Section 4.8 Geoenergy, Helmholtz Centre Potsdam GFZ German Research Centre for Geosciences, Potsdam, Germany, [3]Department of Geosciences, Pennsylvania State University, University Park, PA, USA, [4]College of Earth and Planetary Sciences, University of Chinese Academy of Sciences, Beijing, China

Key Points:

- First direct evidence was found to confirm that surface heat flow is determined by the heat production
- The relationship between natural gamma-ray and heat production is reconstructed
- The formation of rocks with high heat production result from two enrichment processes

Supporting Information:

Supporting Information may be found in the online version of this article.

Correspondence to:

Y. Wang and S. Fuchs,
ybwang@mail.iggcas.ac.cn;
fuchs@gfz-potsdam.de

Citation:

Wang, Y., Furlong, K., Fuchs, S., He, L., & Hu, S. (2023). Terrestrial heat flow variation with depth caused by anomalously high radiogenic heat production. *Geophysical Research Letters*, *50*, e2022GL102312. https://doi.org/10.1029/2022GL102312

Received 29 NOV 2022
Accepted 30 MAR 2023

Author Contributions:

Conceptualization: Yibo Wang, Kevin Furlong, Sven Fuchs
Data curation: Yibo Wang, Sven Fuchs, Shengbiao Hu
Formal analysis: Yibo Wang, Lijuan He
Funding acquisition: Shengbiao Hu
Investigation: Yibo Wang, Shengbiao Hu
Methodology: Yibo Wang, Sven Fuchs
Project Administration: Yibo Wang
Software: Yibo Wang
Supervision: Shengbiao Hu
Validation: Sven Fuchs
Visualization: Yibo Wang, Shengbiao Hu
Writing – original draft: Yibo Wang
Writing – review & editing: Kevin Furlong, Sven Fuchs, Lijuan He

Abstract Surface Heat flow (HF) can be calculated from the accumulation of radiogenic heat production (RHP) of arbitrarily subdivided thin layers of the crust and the residual HF. However, geothermal studies of scientific drilling projects around the world do not have clear vertical correspondence between HF and RHP, which has created a great controversy for the relationship between the two. For the first time, continuous temperature data, thermal conductivity and RHP measurements from the 3,008-m-deep Lujiang-Zongyang Scientific Drilling in the northeastern Yangtze Craton, demonstrate that the abnormal HF is determined by high RHP rock (mean value, 10 μW/m^3). The detailed spatial-temporal study of magmatic activity in the Lujiang-Zongyang basin shows the high RHP rock are concentrated in the early syenite-monzonite period (133–131 Ma) in the northern basin. Two enrichment processes caused by late Neoproterozoic and Mesozoic subduction contribute to the formation.

Plain Language Summary Heat flow (HF) is the most important parameter to characterize the thermal state of the Earth's interior. The surface HF can be calculated from the accumulation of heat production of subdivided thin layers of the crust and residual HF. However, no direct evidence of HF and heat production vertical variation has been found in the present continental scientific drilling wells. In this study, the contribution of the vertical variation of heat production to the surface HF is confirmed for the first time, and the HF values significantly higher than the regional background are determined by the high heat production rock. The study of the genesis of the high heat production rock concluded that they likely underwent two enrichment processes in the Late Neoproterozoic and Mesozoic, respectively, with the Late Mesozoic enrichment process being completed in a very short period of time.

1. Introduction

Heat flow (HF) is the most direct manifestation of the lithospheric thermal state of the surface and provides a strong constraint on the thickness, geophysical properties, and tectonic evolution of the lithosphere. The one-dimensional steady-state conductive geotherms obtained based on the bootstrapping method (Chapman, 1986) assumes that the radiogenic heat production (RHP) can be calculated from the accumulation of RHP of arbitrarily subdivided thin layers, and therefore, the surface HF can be determined by the RHP of the crust and the residual mantle HF. However, the models of the vertical variation of RHP and HF are not reliable due to the very few data constraints and the increased noise in the subsurface. The implementation of continental scientific drilling has made it possible to directly observe the detailed distribution of RHP in the upper crust and opened up the possibility of studying the relationship between HF and the vertical variation of RHP in the crust. The Soviet Union implemented Kola scientific drilling to a maximum depth of 12,262 m; while Germany owned the second deepest ultra-deep scientific drilling Kontinentales Tiefborh programm der Bundesrepublik Deutschland (KTB) in the world with 9.1 km. Since 2001, China has carried out five periods of continental scientific drilling projects, including the first scientific drilling well in Asia, the China Continental Scientific Drilling (CCSD, 5,158 m), and the Cretaceous Continental Scientific Drilling Project in the Songliao Basin (SK-2, 7,018 m).

Several representative scientific drilling projects around the world are selected to study the relationship between HF and RHP in each borehole (Figure 1). As for each borehole, we calculate the HF values at different depths according to Equation 1 and compare them with the vertical variation of HF obtained from the temperature

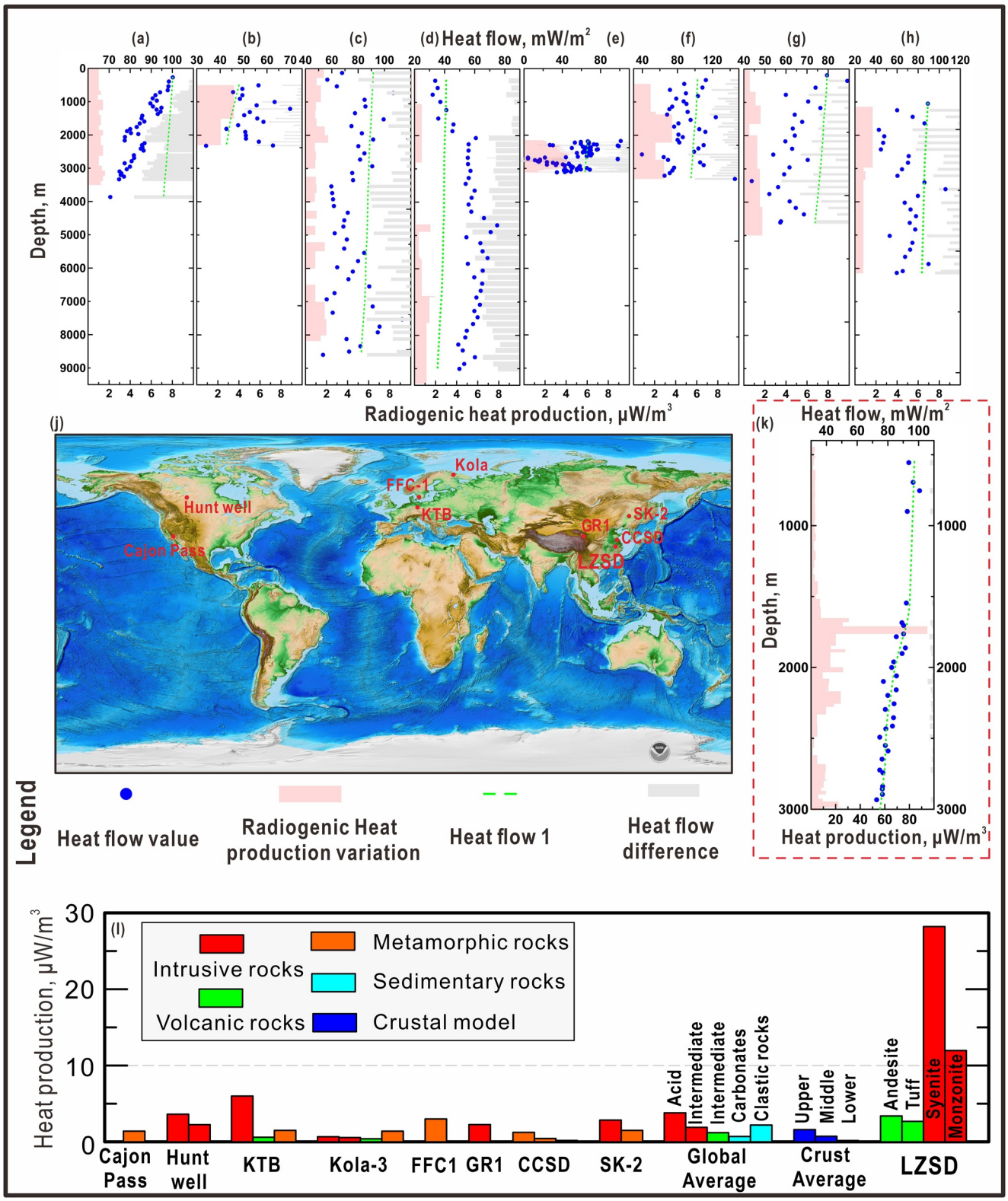

Figure 1.

gradient and thermal conductivity (TC) (HF 1) (Figure 1). Overall, it does not match between the HF variation and HF 1 for each borehole.

$$Q_d = Q_s - \sum Q_A \quad (1)$$

where Q_d denotes the HF value at depth d, Q_A is the sum of the HF generated by the radioactive elements.

In this study, we firstly report the temperature, gradient, and TC and RHP data for samples from the Lujiang-Zongyang Scientific Drilling (LZSD). We determine the variation of the RHP of the LZSD and establish its relationship with the variation of the natural gamma-ray intensity (GR, unit, American Petroleum Institute (API)) value, which simultaneously enhances the reliability of the high RHP well section. We use this to analyze the role of RHP variation in vertical HF change and obtain good correspondence. As a result, the high HF value in the LZSD is determined by the high RHP rock. Finally, we discuss the spatial and temporal distribution, and genesis of the high RHP rock in the Lujiang-Zongyang basin (LZB).

2. Geologic Setting and Methods

The LZB is located in the northeastern section of the Yangtze Craton and east of the Dabie orogenic belt (Figure S1 in the Supporting Information S1). It is a NE-SW trending volcanic basin (Lü et al., 2013). The strata below the Mesozoic volcanic rocks in the LZB can be divided into two parts: (a) the terrigenous clastic rocks and carbonate rocks in the stable continental surface sea environment from Sinian to Middle Triassic; and (b) the terrigenous clastic rocks deposited in the foreland depression area of the Dabie Orogenic Belt during the Late Triassic-Middle Jurassic period (Figures S1 and S2 in the Supporting Information S1). Since the Phanerozoic, the study area has experienced two large-scale tectono-thermal events: the collision between the North China Craton and the Yangtze Craton in the Late Triassic (Li & Li, 2007); sizable regional extension during the Late Mesozoic, accompanied by shallow response represented by basin formation and massive magmatic activity (Wu et al., 2019).

The LZSD is part of the fifth period of Chinese Continental Scientific Drilling, with a borehole depth of 3,008 m. The LZSD is located in Jingbian Village, Qianpu Town, about 37 km northeast of Zongyang County (30.985°N, 117.463°E) (Figure S1 in the Supporting Information S1). The LZSD, the deepest borehole in the LZB and adjacent areas (S. Zhang et al., 2017), began on 21 May 2012, and drilled to the deepest at 3,008.29 m on 9 June 2013.

The LZSD can be divided into three main lithologic layers: 0–1,200 m, early Cretaceous Zhuanqiao Formation, lithology mainly including andesite and tuff; 1,200–1,650 m, the later igneous rock intruded into andesite and tuff with uneven alteration, which is the contact section between the Zhuanqiao Formation and the underlying syenite; 1,650–3,008 m, a deeply concealed intrusion, mainly developing monzonite and syenite. The LZSD constrains the geological structure of the basement in the central basin and provides samples and related data for studying the deep temperature field, the deep tectonic setting of volcanic rock, metallogenic regularity, and the mineralization dynamic process.

Geothermal exploration in the LZB began in the 1970s. Temperature logging and rock thermal property surveys have been carried out in connection with the discovery and exploration of a series of iron-copper-polymetallic deposits in the basin (J. Y. Wang et al., 1981). The published HF data in the LZB and adjacent area has an average HF value of 69.5 ± 13.6 mW/m^2. Most of this geothermal work has been concentrated along the edge of the basin, and temperature measurements are limited to the shallow sedimentary covers with maximum a depth of 400 m.

The LZSD borehole was logged two times, within 10, and 1,874 days (27 July 2018) after the completion of drilling (Figures S2 and S3 in the Supporting Information S1). We have corrected the temperature for different depths using the proposed correction formula (Sass et al., 1992), and the results show that the correction for

Figure 1. Heat flow (HF) and radiogenic heat production (RHP) variation for different scientific drilling projects. (a) Cajon Pass (modified from Sass et al., 1992); (b) Hunt Well (modified from Majorowicz et al., 2014); (c) Kontinentales Tiefborh programm der Bundesrepublik Deutschland (modified from Clauser et al., 1997; Pribnow et al., 2013; Seipold and Huenges, 1998); (d) Kola (modified from Mottaghy et al., 2005; Popov et al., 1999); (e) FFC1 (modified from Rosberg and Erlström, 2021); (f) GR1 (Gonghe Basin) (modified from C. Zhang, 2019); (g) China Continental Scientific Drilling (CCSD) (modified from He et al., 2009); (h) SK-2 (modified from Shi, 2019), (k) Lujiang-Zongyang Scientific Drilling (LZSD) in this research; (l) comparison of RHP in different projects, global average RHP values from Wollenberg and Smith (1987), and crustal model from Y. Huang et al. (2013). HF 1, HF at depth d is calculated from the top via Equation 1; HF difference, the absolute value of the HF difference obtained by the two methods.

temperature is within 1%. The depth lithologically stable section (1,650–2,850) is selected for the calculation of the temperature gradient at 200 m intervals, and the deviation of the gradient values is within 2.5%. Therefore, using the latest temperature measurement data, the requirements of HF calculation and depth temperature field study are fully satisfied. At this point, we consider the borehole temperature in 2018 to be in thermal equilibrium. Based on the steady-state temperature, TC and RHP, we calculated the HF of LZSD and analyzed the correlation between the vertical variation of HF and RHP.

3. Results

3.1. Thermal Conductivity

We collected 147 core samples at intervals of 20–30 m from the top to bottom of LZSD (Table S1 and Figure S4 in the Supporting Information S1). To study the heterogeneity of rock TC, we conducted TC tests for cross-section ($\lambda_{/\!/}$) and longitudinal section ($\lambda_{\perp}$) on 147 core samples (Table S1) (For specific sample preparation and testing methods, refer to J. Wang et al., 2020). Moreover, the anisotropy factor ($K = \lambda_{/\!/}/\lambda_{\perp}$) was calculated (Figure S4 in the Supporting Information S1).

We have collected all the rock types (andesite, syenite, monzonite, tuff, and quartzite) encountered by the LZSD through China Geological Sample Center. The detailed lithologic column is accessible at the China Geological Sample Information, Ministry of Natural Resources of People's Republic of China (http://cgsi.cn/CGSI-Biz/Drill_Show.aspx?DrillID=1669). The measured TC varied from 1.9 to 10.8 W/m/K with a mean value of 3.4 ± 1.7 W/m/K (Table S3 in the Supporting Information S1). The concentrated high TC are likely to be related to the high-strength gypsum and anhydrite veins in the tuff and andesite of the 150–280 m and 1,000–1,500 m sections.

In addition to the mineral composition of the rock, the primary factors affecting TC are pressure, temperature, porosity, and water saturation (Pribnow et al., 2013). We conducted temperature (Sass et al., 1992), water saturation (Roy et al., 1981), and pressure (Seipold & Huenges, 1998) corrections on the samples, respectively. The corrections of pressure- and saturation-corrected TC were within 1% and 3%, respectively. Therefore, we only plot in Figure S4d in the Supporting Information S1 the temperature-corrected TC and the average TC based on the ratio of different corrections. The three corrections offsetting each other to a certain extent in some depths, as a result, the corrected TC is generally smaller than the measured values.

3.2. Radiogenic Heat Production Versus Depth

We measured the concentrations of radioactive heat-producing elements, including uranium (U), thorium (Th), and potassium (K), on 53 core samples (Table S1) (For specific methods, refer to J. Wang et al., 2020). At the same time, we acquired 200–2,500 m GR at an interval of 0.1 m through GR logging (Table S2 in the Supporting Information S1).

The RHP value was calculated through the empirical formula proposed by Rybach (1976):

$$A = 10^{-5}\rho(9.25C_{\mathrm{U}} + 2.56C_{\mathrm{Th}} + 3.48C_{\mathrm{K}}) \quad (2)$$

where A is the RHP (μW/m^3), ρ is the density (kg/m^3), C_{U} and C_{Th} are the U and Th concentrations in ppm, respectively, and C_{K} is the K concentration in percent.

The RHP values vary mainly as a function of lithology. The syenite RHP is in the 6.32–94.44 μW/m^3 range, with an extremely high mean value of 28.21 μW/m^3. The monzonite exhibits large RHP fluctuations, as well as high U and Th concentrations, compared with the andesite and tuff. RHP is in the 1.2–27.7 μW/m^3 range with a mean of 12.0 ± 6.9 (1 SD) μW/m^3 for the monzonite, in the 0.5–3.4 μW/m^3 range, with a mean of 2.4 ± 1.1 μW/m^3 for the andesite, and in the 1.5–3.7 μW/m^3 range with a mean of 2.7 ± 0.7 μW/m^3 for the tuff (Table S3 in the Supporting Information S1). Tuff generally has relatively low U and Th concentrations, resulting in low RHP.

The concentrations of radioactive heat-producing elements of the core samples, along with the GR, were used together to study the RHP variation in the LZSD. We performed regression analysis based on the GR data and measured RHP values. Due to the large range of GR, we established the GR-A empirical Equation 3 ($R^2 = 0.90$) and Equation 4 ($R^2 = 0.74$) for different sections of the LZSD. The RHP calculated from Equations 3 and 4 is in

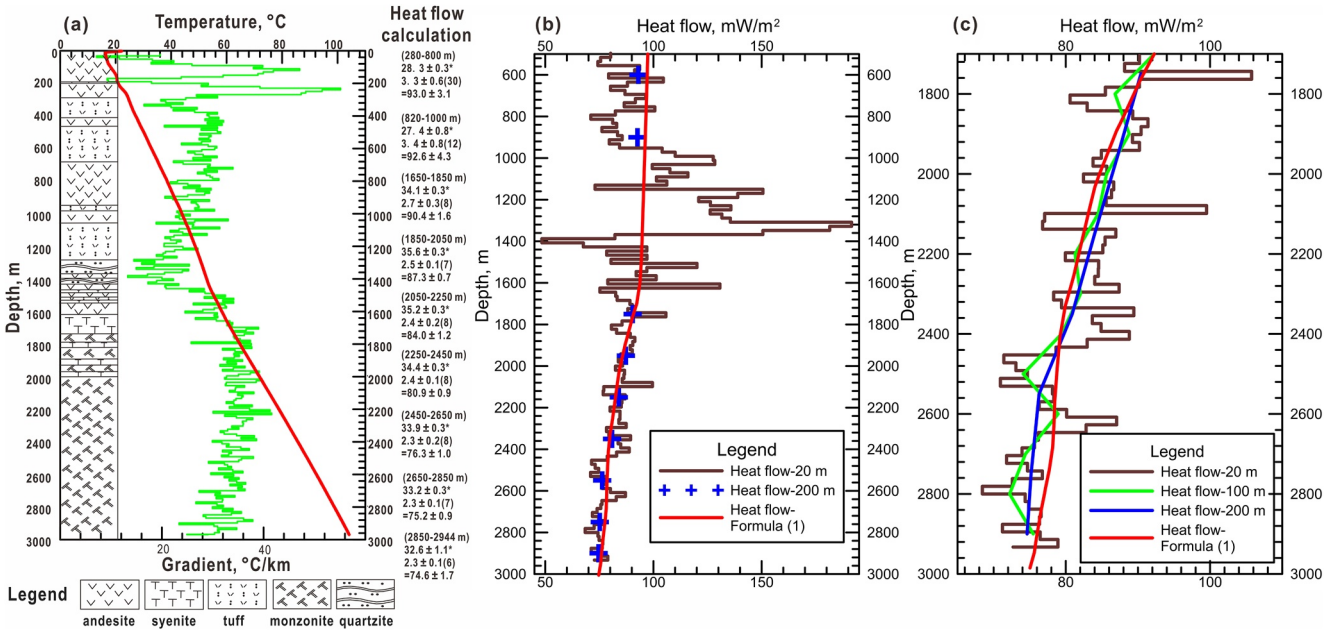

Figure 2. Heat flow (HF) determination and variation in the Lujiang-Zongyang Scientific Drilling (LZSD). The comments on the right side in (a) denote "Gradient ± SD * Thermal conductivity ± SD (number of tests) = Heat flow ± SD"; (b and c) are the HF comparison from different methods for the LZSD.

good agreement with the measured value of the RHP (Figure S5 and Table S4 in the Supporting Information S1, relative error <1%), compared with the results from previous GR-A relationship (Bücker & Rybach, 1996; Luo et al., 2008; Rybach, 1986).

$$A = 0.0383\,[\mathrm{GR\,(API)} - 52.1] \qquad (\mathrm{GR\,(API)} < 250) \tag{3}$$

$$A = 0.0198\,[\mathrm{GR\,(API)} + 332.1] \qquad (\mathrm{GR\,(API)} > 250) \tag{4}$$

Through the study of the RHP, for sections with dramatic API variation, the existing classic formulas may not be effective in calculating the actual RHP. When using the "GR-A" relationship for calculation, special attention should be paid to the scope of the application. For sections with API greater than 250, the measured values should be performed to constrain it.

3.3. Heat Flow Determination and Its Relationship With Heat Production

The HF was calculated via the multiplication of the temperature gradient from the least-squares method with the TC at different depth intervals. The corrected TC was used for the HF determination, with the HF calculated from sections with stable temperature gradient and TC measurements (Figure 2).

The temperature curve above 1,650 m fluctuates greatly with depth, especially in the curve segment above 400 m. The stable gradient and TC yield HF values of 93.0 ± 3.1 mW/m^2 and 92.6 ± 4.3 mW/m^2 at the 280–800 m and 820–1,000 m depth sections, respectively. The HF value is hard to determine in the transition section because of the difficulty in obtaining the accurate bulk TC value in the heterogeneous alteration area. The HF in section 1,560 m to the bottom is determined at intervals of 200 m (Figure 1). The HF of LZSD decreases from top to bottom by approximately 20 mW/m^2.

We calculated the HF values from 500 m to the bottom for the LZSD, at an interval of 20 m (Figure 1). Additionally, vertical HF values were determined in section 1,700–3,000 m to study the relationship between HF and RHP in the relatively stable portion of lithology. The HF values obtained from Equation 1 and the HF calculated in segments as in Figure 1 are in a good agreement, which indicates that the HF variation of LZSD is determined by RHP. The surface HF of LZSD (93 mW/m^2) is much higher than the regional background value due to the presence of a very high RHP rock mass at the depth between 1,650 and 2,980 m. If taking into account the potential depth of the rocks, the background HF can be calculated according to Equation 1, that is, around 68 mW/m^2.

Such large differences indicate that the effect of high RHP rock on the regional HF is significant, and deviations from the background value can reach about 40%.

4. Discussion

4.1. Spatial-Temporal Distribution, Genesis and Tectonic Setting of High RHP Rocks

The RHP of syenite and monzonite in the LZSD is extremely high, which raises new questions: What is the RHP of the LZB? Are there other high RHP rock like the LZSD? Where is its source? Therefore, it is particularly important to understand the spatial and temporal distribution pattern of high RHP rock.

A detailed overview of chronological data, RHP, and spatial and temporal distribution of the rocks in the LZB can be found in Table S5. Depending on the RHP (5 and 10 $\mu W/m^3$ as boundary), deposits are labeled in different colors and thicknesses in Figure S1 in the Supporting Information S1. Almost all magmatic rocks with RHP higher than 5 $\mu W/m^3$ are distributed in the northern LZB, where the host rock is mainly the Zhuanqiao Formation. The RHP of magmatic rocks in different periods varies dramatically, and the timing of high RHP rock is concentrated in the early syenite-monzonite period (129–134 Ma). Similar to the extremely high production of the LZSD, the RHP of Lijiazhuang rock, Qiaochong rock, Longqiao rock, Niutoushan rock, and Liudun rock is above 10 $\mu W/m^3$, with the highest value occurring in the Liudun rock (35.7 $\mu W/m^3$). To clarify the timing for the rocks with high RHP, we summarized the ages of all samples and the corresponding RHP values (Figure 3a). The high-value of RHP mainly appears in 133–131 Ma, which is in the middle of the early syenite-monzonite period.

The RHP of rocks in the LZB are obviously higher than that of the upper crust (1.7 $\mu W/m^3$) (Kemp & Hawkesworth, 2003). Petrological study of the Early Cretaceous magmatism in the LZB, showed that volcanic and intrusive rocks are formed in a similar age (Table S5) and have a close spatial relationship (Figure S1 in the Supporting Information S1), with relatively consistent geochemical characteristics (H. Qiu, 2014; Yuan et al., 2008; S. Zhang et al., 2017), which are the products of different evolutionary stages of homogenous magma (Zhou et al., 2008, 2010), and are considered to belong to the shoshonitic series-intrusive rocks (Jia et al., 2014; S. Zhang et al., 2017).

Geochemical data on magmatic rocks in LZB (Fan et al., 2014; Jia et al., 2014; Yuan et al., 2008; S. Zhang et al., 2017), were collected for studying the magma source of high RHP rock. Nb/U ratios are good evidence for the presence of crustal source material mixing (Hofmann et al., 1986). The Nb/U ratios of the rocks in the LZB are widely distributed but, in the main, significantly lower than those of the mid-ocean ridge basalt and the continental upper crust (Nb/U = 47 and 9, respectively) (Hofmann et al., 1986; Taylor & McLennan, 1995), and close to the Nb/U ratio of fluids retained from the subducted slab (Nb/U = 0.2, less than 0.7) (J. Ayers, 1998). The Nb/U ratio of high RHP rock is between 0.5 and 1.9 (Figure 3b), and the lower ratio implies that they are more strongly influenced by fluid metasomatism. In addition, including high RHP rock, Nb/Ta-La/Yb diagram in the LZB does not have negative correlation characteristics, indicating that the rocks do not have crustal mixing (Figure 3c) (Münker, 1998). The mixed lithosphere-asthenospheric mantle and lithospheric mantle are considered to be the main source regions of the magmatic rocks in the LZB, based on an interpretation derived from the La/Yb-Nb/La diagram (Abdel-Rahman & Nassar, 2004) (Figure 3d). However, high RHP rock have significantly higher Nb/La ratios, indicating an asthenospheric mantle and mixed lithosphere-asthenospheric mantle source region signature.

The trace element signature of high RHP rock has a Nb/U ratio similar to that of fluids released from the subduction zone (Figure 3b), and the Pb-Pb/Ce diagram also indicates the influence of deep-sea sediments on the magma source area (Figure 3e), which likely indicates an enrichment process in the regional lithospheric mantle during the Mesozoic, when the Izanagi plate subducted to the Eurasian plate and the fluids generated by the dehydration of the oceanic crust may lead to mantle metasomatism.

However, it is unlikely that mantle-derived magma is the only component that produces high RHP rock in a very short period time (Figure 3). In addition, the volcanic rocks in the LZB are characterized by enrichment not only in fluid-mobile trace elements (e.g., Rb, Ba, and Pb) but also in melt-mobile trace elements (e.g., Th and LREE). In summary, the required metasomatic agent would have more Th, U, and LREE content than suggested by experimental studies (J. C. Ayers et al., 1997; Brenan et al., 1995; Kessel et al., 2005; Plank, 2005).

Based on Pb, Nd and Hf isotopic studies, an enriched lithospheric mantle was formed by the fluid metasomatic released from oceanic sediments due to the subduction of the Cathaysia plate to the Yangtze in the middle-late

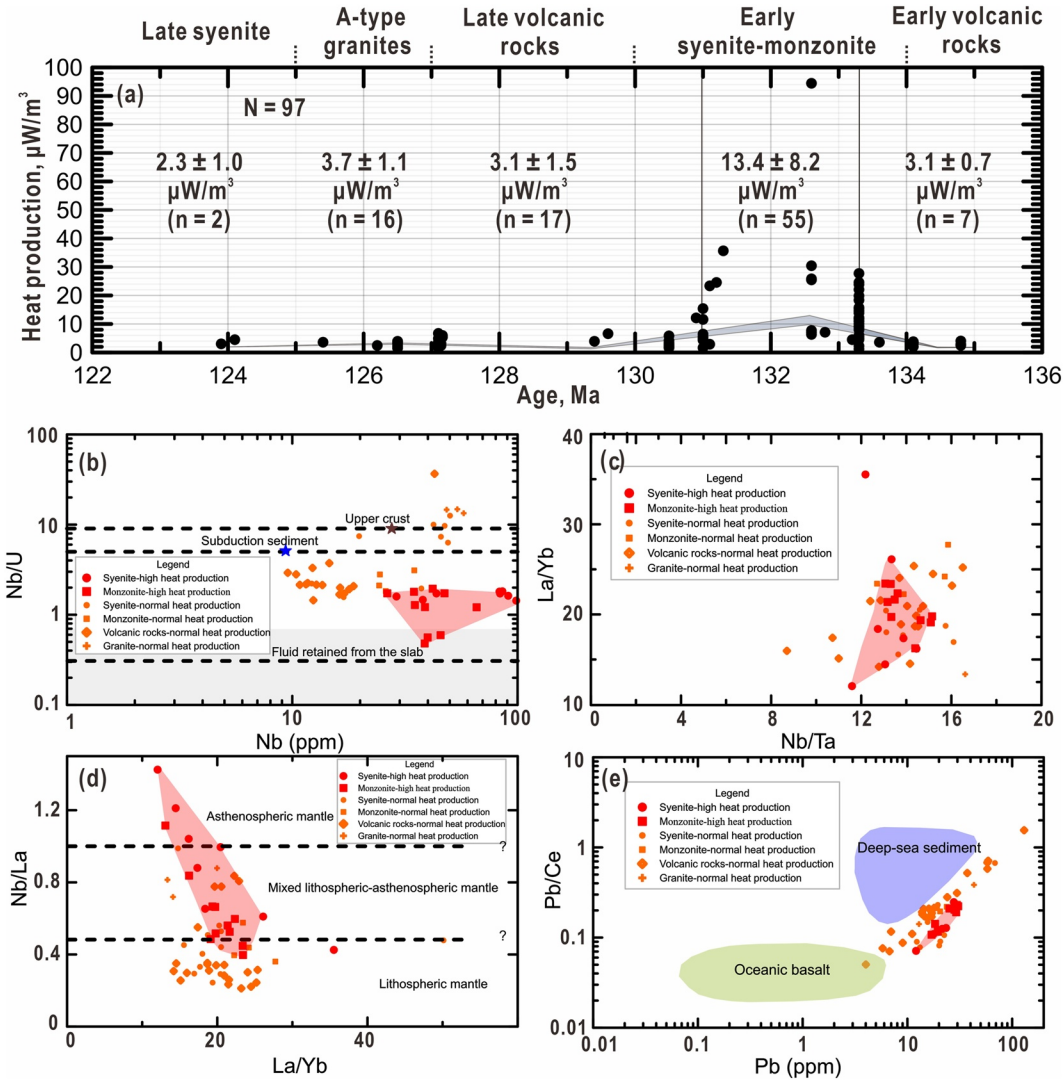

Figure 3. (a) Radiogenic heat production (RHP) values from different periods in the Lujiang-Zongyang basin (LZB) are plotted as a function of ages; (b–e) illustration of the classification of trace elements in rocks in the LZB. The lower bound of the shaded region in (a) is defined by the binned median of the RHP, and the upper bound by the binned average (Table S5). (b) Nb-Nb/U diagram; (c) Nb/Ta-La/Yb diagram; (d) La/Yb-Nb/La diagram (after Abdel-Rahman and Nassar, 2004); (e) Pb-Pb/Ce diagram (after Othman et al., 1989). The rocks with RHP, higher than 5 μW/m^3 are classified as high RHP rock in red color; the red shadow regions are the distributions of the high RHP rocks in the LZB.

Proterozoic (Chen et al., 2014; Xue et al., 2010; Yan et al., 2005; S. Zhang et al., 2017), which is the main mechanism responsible for the source mixing of oceanic and continental arc magmatism (Tatsumi, 2006).

As mentioned above, geochemical signatures suggest a large number of sediment components incorporated into the magmatic source of the magmatic rocks in the LZB. Combined with the tectonic evolution of South China (Charvet, 2013) and the paleogeographic reconstruction of the (paleo) Pacific plate (Müller et al., 2016), we consider the two enrichment processes can be well explained by the Neoproterozoic and Late Mesozoic subduction. During the Greenwich period, the subduction of the Cathaysia oceanic plate beneath the Yangtze Craton was the most likely tectonic event for this source mixing. The first enrichment occurred when sediment-generated melt would rise into the overlying mantle wedge and then react with wedge peridotite to form metasomes. As part of the new continental lithospheric mantle, these metasomes can be stored at the base of the lithosphere for hundreds of million years due to the unique stability of the South China Plate in the period between the Late Neoproterozoic and Early Mesozoic (Qi et al., 2016). In the early Cretaceous, the metasomes were partially melted by heating due to the lithospheric extension of the Lower Yangtze Craton caused by the subduction of the

Izanagi plate, producing the shoshonitic series-intrusive rocks of the LZB (Jia et al., 2014; S. Zhang et al., 2017). The emergence of high RHP rock corresponds to the onset of strong regional extension, and the peak of craton destruction in the Lower Yangtze Craton was slightly earlier than that in the North China Craton, which is also evidenced by HF (N. Qiu et al., 2015; J. Wang et al., 2020, 2021), igneous activity (Wu et al., 2019), and extensional deformation (Lin et al., 2013).

4.2. Vertical Variations of Radiogenic Heat Production and Heat Flow for Global Scientific Drilling Projects

The absence of a good correlation of vertical changes between HF and RHP in continental scientific drilling projects worldwide may be due to three factors: first, the influence of signals of climate change, such as Hunt Well in Canada (Majorowicz et al., 2014), KTB in Germany (Clauser et al., 1997; Pribnow et al., 2013), and Kola-3 in Russia (Mottaghy et al., 2005; Popov et al., 1999), mainly manifested by the gradual increase of HF with depth at shallow depths (shallower than 1–2 km); second, the redistribution of heat at shallow depths, such as the effect of groundwater activity; and third, the difficulty of obtaining geothermal data (temperature, TC and RHP data, etc.) at high resolution.

The LZSD belongs to the South China Plate in East Asia, and the previous paleoclimate study indicate that the region was very limited (within −2°C) affected by the Last Glacial Maximum, which differs significantly from the impact on Europe and the North America (Jiang et al., 2011; Osman et al., 2021; Seltzer et al., 2021; Tierney et al., 2020). Another China Continental Scientific Drilling CCSD ∼500 km away from the LZSD also has no significant paleoclimate record (the HF at the shallow (200–500 m) owns the highest value in CCSD), which is also corroborated by the inversion methods of obtaining the climate signal in this region under the attempts of S. P. Huang et al. (2008) and us. In contrast, the scientific projects Kola and Hunt Well are affected by Last Glacial Maximum obviously (Majorowicz et al., 2014; Mottaghy et al., 2005; Popov et al., 1999).

The shallow HF in LZSD is as high as 93 mW/m^2 (∼600 m) and gradually decreases to 75 mW/m^2 at the bottom of the borehole at ∼2,900 m (Figure 2). The huge HF variation is very unusual and the high RHP can constrain the HF very well. The RHP value in LZSD is extremely high compared to those of other scientific projects, with an average RHP value of 28 μW/m^3 for the syenite and 12 μW/m^3 for the monzonite, which are higher than the global average value of acidic intrusive rocks (3.8 μW/m^3) (Wollenberg & Smith, 1987), significantly higher than the RHP value of the upper crust (1.6 μW/m^3) (Y. Huang et al., 2013), and dramatically different from that of the intrusive rocks of other scientific projects (e.g., 2.3–3.6 μW/m^3 for the Hunt Well, granite (Majorowicz et al., 2014); a maximum of 6.0 μW/m^3 for the KTB granite (Clauser et al., 1997; Pribnow et al., 2013); and only 0.7 μW/m^3 for the basal intrusive rocks of Kola (Mottaghy et al., 2005; Popov et al., 1999)) (Figure 1l). In addition, the volcanic rocks of LZSD also have higher RHP values than those of other global scientific drilling projects (Figure 1l). On the one hand, the previous discussion shows that the genesis of high RHP in LZSD is regional and large-scale enough; on the other hand, in LZSD, the vertical variation of (high) RHP is also supported by fine geophysical results (logging parameters, such as, GR data in this research; geophysical profiles from Dong et al., 2010; S. Zhang et al., 2017), which makes it reasonable to assume that the high surface HF values in LZSD are determined by the vertical variation of high RHP. At the same time, it is a matter of interest whether the rock mass with high RHP is an important sensitivity parameter to explore the relationship between the two in practical. We look forward to more research results on this in the future.

5. Conclusions

So far, it is rather rare to see a good match between the variation of the HF and the RHP in most deep boreholes, but it cannot be denied the contribution of the RHP to the surface HF (Jones, 1987; Perry et al., 2006). The vertical change of HF and RHP in the LZSD is well coupled, suggesting that an elevated crustal radioactive component in the LZSD is largely responsible for the high HF.

The new "GR-A" empirical formula for the LZSD is proposed: compared with the measured RHP values, the overall error is less than 1%. The HF at depth near 600 and 900 m are 93.0 and 92.6 mW/m^2, respectively. The measured HF values at the LZSD decrease gradually from 90.4 mW/m^2 at a depth of 1,700 m to 74.6 mW/m^2 near the bottom of the borehole.

The high RHP rock come from the early syenite-monzonite period (133–131 Ma) in the northern LZB. High RHP rock can be a result of two enrichment processes brought on by late Neoproterozoic and Mesozoic subduction.

Data Availability Statement

The data supporting the conclusions of this paper can be downloaded from online database: https://doi.org/10.6084/m9.figshare.22362622.

Acknowledgments
We thank SinoProbe Group very much, who provided geophysical logging data of the LZSD that are important for our RHP and geothermal field analysis. We thank the China Geological Sample Information, Ministry of Natural Resources of the People's Republic of China, for its assistance in measuring TC. We are grateful to Donggang Nie and Kesong Zhang from Anhui Geological Prospecting Bureau, Zhuting Wang from China University of Mining and Technology, for their help in logging. This research was accomplished under the support of the National Key R&D Program of China (Grant 2021YFA0716003), the National Natural Science Foundation of China (Grant 42074096), the State Key Laboratory of Lithospheric Evolution (SKL-K202104), and the China Scholarship Council (CSC NO. 202104910163).

References

Abdel-Rahman, A.-F. M., & Nassar, P. E. (2004). Cenozoic volcanism in the Middle East: Petrogenesis of alkali basalts from northern Lebanon. *Geological Magazine*, *141*(5), 545–563. https://doi.org/10.1017/S0016756804009604

Ayers, J. (1998). Trace element modeling of aqueous fluid–peridotite interaction in the mantle wedge of subduction zones. *Contributions to Mineralogy and Petrology*, *132*(4), 390–404. https://doi.org/10.1007/s004100050431

Ayers, J. C., Dittmer, S. K., & Layne, G. D. (1997). Partitioning of elements between peridotite and H2O at 2.0–3.0 GPa and 900–1100°C, and application to models of subduction zone processes. *Earth and Planetary Science Letters*, *150*(3–4), 381–398. https://doi.org/10.1016/s0012-821x(97)00096-4

Brenan, J. M., Shaw, H. F., & Ryerson, F. J. (1995). Experimental evidence for the origin of lead enrichment in convergent-margin magmas. *Nature*, *378*(6552), 54–56. https://doi.org/10.1038/378054a0

Bücker, C., & Rybach, L. (1996). A simple method to determine heat production from gamma-ray logs. *Marine and Petroleum Geology*, *13*(4), 373–375. https://doi.org/10.1016/0264-8172(95)00089-5

Chapman, D. (1986). Thermal gradients in the continental crust. *Geological Society, London, Special Publications*, *24*(1), 63–70. https://doi.org/10.1144/GSL.SP.1986.024.01.07

Charvet, J. (2013). The Neoproterozoic–early Paleozoic tectonic evolution of the South China Block: An overview. *Journal of Asian Earth Sciences*, *74*, 198–209. https://doi.org/10.1016/j.jseaes.2013.02.015

Chen, L., Zhao, Z.-F., & Zheng, Y.-F. (2014). Origin of andesitic rocks: Geochemical constraints from Mesozoic volcanics in the Luzong basin, South China. *Lithos*, *190*, 220–239. https://doi.org/10.1016/j.lithos.2013.12.011

Clauser, C., Giese, P., Huenges, E., Kohl, T., Lehmann, H., Rybach, L., et al. (1997). The thermal regime of the crystalline continental crust: Implications from the KTB. *Journal of Geophysical Research*, *102*(B8), 18417–18441. https://doi.org/10.1029/96JB03443

Dong, S., Xiang, H., Gao, R., Lv, Q., Li, J., Zhan, S., et al. (2010). Deep structure and ore formation with in Lujiang-Zongyang volcanic ore concentrated area in Middle to Lower Reaches of Yangtze River. *Acta Petrologica Sinica*, *26*, 2529–2542. (in Chinese With English Abstract). https://doi.org/10.2113/gssajg.113.3.241

Fan, Y., Qiu, H., Zhou, T., Yuan, F., & Zhang, L. (2014). LA-ICP MS Zircon U-Pb dating for the hidden intrusions in the Lu-Zong Basin and its tectonic significance. *Acta Geologica Sinica*, *88*, 532–546. (in Chinese With English Abstract). https://doi.org/10.19762/j.cnki.dizhixuebao.2014.04.008

He, L., Hu, S., Yang, W., & Wang, J. (2009). Radiogenic heat production in the lithosphere of Sulu ultrahigh-pressure metamorphic belt. *Earth and Planetary Science Letters*, *277*(3–4), 525–538. https://doi.org/10.1016/j.epsl.2008.11.022

Hofmann, A. W., Jochum, K. P., Seufert, M., & White, W. M. (1986). Nb and Pb in oceanic basalts: New constraints on mantle evolution. *Earth and Planetary Science Letters*, *79*(1–2), 33–45. https://doi.org/10.1016/0012-821X(86)90038-5

Huang, S. P., Pollack, H. N., & Shen, P. Y. (2008). A late Quaternary climate reconstruction based on borehole heat flux data, borehole temperature data, and the instrumental record. *Geophysical Research Letters*, *35*(13), L13703. https://doi.org/10.1029/2008GL034187

Huang, Y., Chubakov, V., Mantovani, F., Rudnick, R. L., & McDonough, W. F. (2013). A reference Earth model for the heat-producing elements and associated geoneutrino flux. *Geochemistry, Geophysics, Geosystems*, *14*(6), 2003–2029. https://doi.org/10.1002/ggge.20129

Jia, L., Xu, W., Lv, Q., Mo, X., Xiong, X., Li, J., & Wang, L. (2014). LA-MC-ICP MS zircon U-Pb geochronology and petrological geochemistry of scientific deep drilling in Zhuanqiao, Lujiang-Zongyang volcanic basin. *Acta Petrologica Sinica*, *30*, 995–1016. (in Chinese With English Abstract). https://doi.org/10.1127/0078-0421/2014/0044

Jiang, D., Lang, X., Tian, Z., & Guo, D. (2011). Last glacial maximum climate over China from PMIP simulations. *Palaeogeography, Palaeoclimatology, Palaeoecology*, *309*(3–4), 347–357. https://doi.org/10.1016/j.palaeo.2011.07.003

Jones, M. Q. W. (1987). Heat flow and heat production in the Namaqua Mobile Belt, South Africa. *Journal of Geophysical Research*, *92*(B7), 6273–6289. https://doi.org/10.1029/JB092iB07p06273

Kemp, A., & Hawkesworth, C. (2003). Granitic perspectives on the generation and secular evolution of the continental crust. In R. L. Rudnick (Ed.), *The crust. Treatise on geochemistry, 3* (pp. 349–410). Elsevier. https://doi.org/10.1016/B0-08-043751-6/03027-9

Kessel, R., Schmidt, M. W., Ulmer, P., & Pettke, T. (2005). Trace element signature of subduction-zone fluids, melts and supercritical liquids at 120–180 km depth. *Nature*, *437*(7059), 724–727. https://doi.org/10.1038/nature03971

Li, Z. X., & Li, X. H. (2007). Formation of the 1300-km-wide intracontinental orogen and postorogenic magmatic province in Mesozoic South China: A flat-slab subduction model. *Geology*, *35*(2), 179–182. https://doi.org/10.1130/G23193A.1

Lin, W., Charles, N., Chen, Y., Chen, K., Faure, M., Wu, L., et al. (2013). Late Mesozoic compressional to extensional tectonics in the Yiwulüshan massif, NE China and their bearing on the Yinshan–Yanshan orogenic belt. *Gondwana Research*, *23*(1), 78–94. https://doi.org/10.1016/J.GR.2012.02.012

Lü, Q., Yan, J., Shi, D., Dong, S., Tang, J., Wu, M., & Chang, Y. (2013). Reflection seismic imaging of the Lujiang–Zongyang volcanic basin, Yangtze Metallogenic Belt: An insight into the crustal structure and geodynamics of an ore district. *Tectonophysics*, *606*, 60–77. https://doi.org/10.1016/j.tecto.2013.04.006

Luo, M., Pan, H., Zhao, Y., Zhang, H., & Zhou, F. (2008). Natural radioactivity logs and interpretation from the CCSD main hole. *Journal of Earth Science*, *33*, 661–671. (in Chinese With English Abstract). https://doi.org/10.3799/dqkx.2008.081

Majorowicz, J., Chan, J., Crowell, J., Gosnold, W., Heaman, L. M., Kück, J., et al. (2014). The first deep heat flow determination in crystalline basement rocks beneath the Western Canadian Sedimentary Basin. *Geophysical Journal International*, *197*(2), 731–747. https://doi.org/10.1093/gji/ggu065

Mottaghy, D., Schellschmidt, R., Popov, Y. A., Clauser, C., Kukkonen, I. T., Nover, G., et al. (2005). New heat flow data from the immediate vicinity of the Kola super-deep borehole: Vertical variation in heat flow confirmed and attributed to advection. *Tectonophysics*, *401*(1–2), 119–142. https://doi.org/10.1016/j.tecto.2005.03.005

Müller, R. D., Seton, M., Zahirovic, S., Williams, S. E., Cannon, J., Wright, N. M., et al. (2016). Ocean basin evolution and global-scale plate reorganization events since Pangea breakup. *Annual Review of Earth and Planetary Sciences*, *44*(1), 107–138. https://doi.org/10.1146/annurev-earth-060115-012211

Münker, C. (1998). Nb/Ta fractionation in a Cambrian arc/back arc system, New Zealand: Source constraints and application of refined ICPMS techniques. *Chemical Geology*, *144*(1–2), 23–45. https://doi.org/10.1016/S0009-2541(97)00105-8

Osman, M. B., Tierney, J. E., Zhu, J., Tardif, R., Hakim, G. J., King, J., & Poulsen, C. J. (2021). Globally resolved surface temperatures since the Last Glacial Maximum. *Nature*, *599*(7884), 239–244. https://doi.org/10.1038/s41586-021-03984-4

Othman, D. B., White, W. M., & Patchett, J. (1989). The geochemistry of marine sediments, island arc magma genesis, and crust-mantle recycling. *Earth and Planetary Science Letters*, *94*(1–2), 1–21. https://doi.org/10.1016/0012-821X(89)90079-4

Perry, H. K. C., Jaupart, C., Mareschal, J. C., & Bienfait, G. (2006). Crustal heat production in the Superior Province, Canadian Shield, and in North America inferred from heat flow data. *Journal of Geophysical Research*, *111*(B4), B04401. https://doi.org/10.1029/2005jb003893

Plank, T. (2005). Constraints from thorium/lanthanum on sediment recycling at subduction zones and the evolution of the continents. *Journal of Petrology*, *46*(5), 921–944. https://doi.org/10.1093/petrology/egi005

Popov, Y. A., Pevzner, S. L., Pimenov, V. P., & Romushkevich, R. A. (1999). New geothermal data from the Kola superdeep well SG-3. *Tectonophysics*, *306*(3–4), 345–366. https://doi.org/10.1016/S0040-1951(99)00065-7

Pribnow, D., Williams, C. F., Sass, J. H., & Keating, R. (2013). Thermal conductivity of water–saturated rocks from the KTB Pilot Hole at temperatures of 25 to 300°C. *Geophysical Research Letters*, *23*(4), 391–394. https://doi.org/10.1029/95GL00253

Qi, Y., Hu, R., Liu, S., Coulson, I. M., Qi, H., Tian, J., & Zhu, J. (2016). Petrogenesis and geodynamic setting of Early Cretaceous mafic–ultramafic intrusions, South China: A case study from the Gan–Hang tectonic belt. *Lithos*, *258*, 149–162. https://doi.org/10.1016/j.lithos.2016.04.027

Qiu, H. (2014). *Diagenesis of intermediate-acidic intrusive rock in the Luzong areas, Anhui Province*. Hefei University of Technology. (in Chinese With English Abstract).

Qiu, N., Wei, X., Zuo, Y., & Jian, C. (2015). Meso–Cenozoic thermal regime in the Bohai Bay Basin, eastern North China Craton. *International Geology Review*, *57*(3), 271–289. https://doi.org/10.1080/00206814.2014.1002818

Rosberg, J. E., & Erlström, M. (2021). Evaluation of deep geothermal exploration drillings in the crystalline basement of the Fennoscandian Shield Border Zone in south Sweden. *Geothermal Energy*, *9*(1), 1–25. https://doi.org/10.1186/s40517-021-00203-1

Roy, R. F., Beck, A. E., & Touloukian (1981). Thermophysical properties of rocks. *Physical Properties of Rocks and Minerals*, *2*, 409–502. https://doi.org/10.1080/00206814.2014.1002818

Rybach, L. (1976). Radioactive heat production in rocks and its relation to other petrophysical parameters. *Pure and Applied Geophysics*, *114*(2), 309–317. https://doi.org/10.1007/BF00878955

Rybach, L. (1986). Amount and significance of radioactive heat sources in sediments'. In J. Burrus (Ed.), *Thermal modeling in sedimentary basins* (pp. 311–322). Editions Technip.

Sass, J. H., Lachenbruch, A. H., Moses, T. H., & Morgan, P. (1992). Heat flow from a scientific research well at Cajon Pass, California. *Journal of Geophysical Research*, *97*(B4), 5017–5030. https://doi.org/10.1029/91JB01504

Seipold, U., & Huenges, E. (1998). Thermal properties of gneisses and amphibolites—High pressure and high temperature investigations of KTB–rock samples. *Tectonophysics*, *291*(1–4), 173–178. https://doi.org/10.1016/S0040-1951(98)00038-9

Seltzer, A. M., Ng, J., Aeschbach, W., Kipfer, R., Kulongoski, J. T., Severinghaus, J. P., & Stute, M. (2021). Widespread six degrees Celsius cooling on land during the Last Glacial Maximum. *Nature*, *593*(7858), 228–232. https://doi.org/10.1038/s41586-021-03467-6

Shi, Y. (2019). *Lithospheric thermal structure and geothermal resource of Northern Songliao Basin, NE China*. University of Chinese Academy of Sciences.

Tatsumi, Y. (2006). High-Mg andesites in the Setouchi volcanic belt, southwestern Japan: Analogy to Archean magmatism and continental crust formation? *Annual Review of Earth and Planetary Sciences*, *34*(1), 467–499. https://doi.org/10.1146/annurev.earth.34.031405.125014

Taylor, S. R., & McLennan, S. M. (1995). The geochemical evolution of the continental crust. *Reviews of Geophysics*, *33*(2), 241–265. https://doi.org/10.1029/95RG00262

Tierney, J. E., Zhu, J., King, J., Malevich, S. B., Hakim, G. J., & Poulsen, C. J. (2020). Glacial cooling and climate sensitivity revisited. *Nature*, *584*(7822), 569–573. https://doi.org/10.1038/s41586-020-2617-x

Wang, J. Y., Chen, M. X., Wang, J. A., Deng, X., Wang, J., Shen, H. C., et al. (1981). Geothermal studies in China. *Journal of Volcanology and Geothermal Research*, *9*(1), 57–76. https://doi.org/10.1016/0377-0273(81)90014-7

Wang, Y., Bai, Y., Wang, L., Guan, J., Wang, Y., Wang, Z., et al. (2021). Exploration process and genesis mechanism of deep geothermal resources in the North Jiangsu Basin, East China: From nothing to something. *Frontiers in Earth Science*, *9*, 1242. https://doi.org/10.3389/feart.2021.784600

Wang, Y., Hu, D., Wang, L., Guan, J., Bai, Y., Wang, Z., et al. (2020). The present-day geothermal regime of the North Jiangsu Basin, East China. *Geothermics*, *88*, 101829. https://doi.org/10.1016/j.geothermics.2020.101829

Wollenberg, H. A., & Smith, A. R. (1987). Radiogenic heat production of crustal rocks: An assessment based on geochemical data. *Geophysical Research Letters*, *14*(3), 295–298. https://doi.org/10.1029/gl014i003p00295

Wu, F., Yang, J., Xu, Y., Wilde, S. A., & Walker, R. J. (2019). Destruction of the North China Craton in the Mesozoic. *Annual Review of Earth and Planetary Sciences*, *47*(1), 173–195. https://doi.org/10.1146/annurev-earth-053018-060342

Xue, H., Dong, S., & Ma, F. (2010). Geochemistry of shoshonitic volcanic rocks in the Luzong basin, Anhui Province (eastern China): Constraints on Cretaceous lithospheric thinning of the Lower Yangtze Region. *Acta Geologica Sinica*, *84*, 664–681. https://doi.org/10.1017/S0004972710001772

Yan, J., Chen, J., Xie, Z., Yang, G., Yu, G., & Qian, H. (2005). Geochemistry of Late Mesozoic basalts from Kedoushan in the Middle and Lower Yangtze regions: Constraints on characteristics and evolution of the lithospheric mantle. *Geochimica*, *34*, 455–469. https://doi.org/10.3321/j.issn:0379-1726.2005.05.004

Yuan, F., Zhou, T., Fan, Y., Lu, S., Qian, C., Zhang, L., et al. (2008). Source, evolution and tectonic setting of Mesozoic volcanic rocks in Luzong basin, Anhui Province. *Acta Petrologica Sinica*, *24*, 1691–1702. (in Chinese With English Abstract).

Zhang, C. (2019). *Geothermal characteristics and genesis mechanism of Hot Dry Rock geothermal resources of Gonghe basin, northeastern Tibetan Plateau*. University of Chinese Academy of Sciences.

Zhang, S., Zhou, T., Wu, M. A., Zhang, Z., Xue, H., & Li, X. (2017). Geochronology and petrological geochemistry of Intrusions in the Lujiang-Zongyang Basin in the mineralization belt of the middle and lower reaches of Yangtze River revealed by Scientific Drilling. *Acta Geologica Sinica*, *91*, 1483–1505. (in Chinese With English Abstract). https://doi.org/10.19762/j.cnki.dizhixuebao.2017.07.006

Zhou, T., Fan, Y., Yuan, F., Sanming, L. U., Shang, S., Cooke, D., et al. (2008). Geochronology of the volcanic rocks in the Lu-Zong basin and its significance. *Science in China Series D: Earth Sciences*, *51*(10), 112–124. https://doi.org/10.1007/s11430-008-0111-7

Zhou, T., Fan, Y., Yuan, F., Song, C., Zhang, L., Qian, C., et al. (2010). Temporal-spatial framework of magmatic intrusions in Luzong volcanic basin in East China and their constrain to mineralizations. *Acta Petrologica Sinica*, *26*, 2694–2714. (in Chinese With English Abstract).

References From the Supporting Information

Du, X. (2018). *Discussion on genesis of A-type granite in southern Luzong basin, Anhui Province*. Hefei University of Technology. (in Chinese With English Abstract). https://doi.org/10.12017/dzkx.2018.037

Fan, Y., Zhou, T. F., Yuan, F., Qian, C. C., & Cooke, D. R. (2008). LA-ICP-MS zircon U-Pb ages of the A-type granites in the Lu-Zong (Lujiang-Zongyang) area and their geological significances. *Acta Petrologica Sinica*, *24*, 1715–1724. (in Chinese With English Abstract).

Li, H., Zhang, R., & Hu, S. (2009). Geochemical characteristics of syenite and its genesis in the Luzong basin. *Journal of Jilin University*, *39*, 839–848. (in Chinese With English Abstract). https://doi.org/10.3969/j.issn.1671-5888.2009.05.012

Lü, Q., Shi, D., Liu, Z., Zhang, Y., Dong, S., & Zhao, J. (2015). Crustal structure and geodynamic of the Middle and Lower reaches of Yangtze metallogenic belt and neighboring areas: Insights from deep seismic reflection profiling. *Journal of Asian Earth Sciences*, *114*, 704–716. https://doi.org/10.1016/j.jseaes.2015.03.022

Wang, Q., Wyman, D. A., Xu, J., Zhao, Z., Jian, P., Xiong, X., et al. (2006). Petrogenesis of Cretaceous adakitic and shoshonitic igneous rocks in the Luzong area, Anhui Province (eastern China): Implications for geodynamics and Cu–Au mineralization. *Lithos*, *89*(3–4), 424–446. https://doi.org/10.1016/j.lithos.2005.12.010

Wei, G., Zhang, Z., Wu, M., Shu, Z., & Cai, X. (2017). Chronological study of the concealed intrusions in Fanshan Area, Lujiang-Zongyang volcanic basin, Anhui Province. *Modern Mining*, *580*(8), 29–35. (in Chinese With English Abstract). https://doi.org/10.3969/j.issn.1674-6082.2017.08.006

Zhang, L. (2011). *Polymetallic mineralisation and associated magmatic and volcanic activity in the Luzong basin, Anhui Province, eastern China*. Hefei University of Technology. (in Chinese With English Abstract). https://doi.org/10.7666/d.y2041689